Quantitative Ultrasound Estimates From Populations of Scatterers With Continuous Size Distributions

Roberto Lavarello, *Member, IEEE*, and Michael Oelze, *Senior Member, IEEE*

***Abstract*—Although quantitative ultrasound imaging based on backscattering coefficients has proven potential for tissue characterization, the scattering models used in most studies assume distributions of identical scatterers. However, actual tissues may exhibit multiple levels of spatial scales. Therefore, the objective of the present study is to analyze the effects of scatterer size distributions when using a fluid-sphere model for estimating values of effective scatterer diameter (ESD) through both simulations and experiments. For simulations, ESD estimates were obtained at several analysis frequencies between 1 and 40 MHz from populations of scatterers with diameters ranging between 25 and 100 μm, 25 and 50 μm, 50 and 100 μm, and 50 and 75 μm. For sufficiently high analysis frequencies, the ESD estimates obtained through simulations were approximately inversely proportional to frequency and mostly independent of the underlying scatterer size distribution. Asymptotic expressions for the expected ESD estimates at low- and high-frequency limits were derived. Experiments were conducted using two gelatin phantoms with contrast agent spheres ranging in diameter from 30 to 140 μm and 70 to 140 μm, and 5-, 7.5-, 10-, and 13-MHz focused transducers. Not only was the asymptotic behavior of ESD versus frequency estimates observed experimentally, but also the experimental ESD estimates using the 10- and 13-MHz transducers were lower than the smallest scatterers present in the second phantom. These results may have a direct impact on how scatterer size estimates corresponding to specimens with different subresolution spatial scales should be interpreted.**

I. Introduction

Quantitative ultrasound imaging based on backscattering coefficients (referred to in this work as QUS) has proven potential for tissue characterization. Experimental work in the literature includes explorations of ocular lesions [1], prostate [2], kidney [3], liver [4], and rat mammary tumors [5], among others. Microstructural information is obtained by assuming that a large number of scatterers per resolution cell exist and that incoherent scattering dominates the backscattered power spectrum. If multiple scattering is neglected, the backscattered spectrum estimates can be fitted to a parametric model that represents how a single scatterer radiates sound as a function of frequency. The property of interest in this study is the effective scatterer diameter (ESD), which represents the typical size of unresolvable scatterers within the insonified region.

Although many efforts have been conducted to improve the performance of ESD estimation, including spectral smoothing [6], angular compounding [7], and attenuation estimation and compensation [8], only a few studies have dealt with the fact that a single-size scatterer model may not properly represent backscattering from complex structures with different spatial scales. Some researchers have studied the effects of scatterer size variations when obtaining ESD estimates using Bernoulli (i.e., a population consisting of scatterers of two different sizes) [9], [10] and Gaussian [11], [12] size distributions.

For Bernoulli size distributions, Roberjot *et al.* [9] studied the case in which the concentration of small scatterers was significantly higher than that of the large scatterers. The investigators used a solid sphere scattering model [13] to obtain estimates of scatterer size from a physical phantom containing glass beads. The size of the smallest and largest beads were around 4 μm and between 75 and 90 μm, respectively. Roberjot *et al.* obtained experimental ESD estimates of 96, 28, and 8 μm when using analysis frequencies between 2 and 8, 8 and 30, and 34 and 60 MHz, respectively. The authors concluded that different frequency ranges were more sensitive to different spatial scales, and that in particular higher frequencies were more sensitive to smaller scatterers. Mamou *et al.* [10] studied the effects of varying the acoustic concentration of the individual sub-populations using a fluid sphere scattering model. They concluded that to resolve the smaller scatterers, either the number density or acoustic impedance mismatch of the smaller scatterers must be greater than the corresponding values for the larger scatterers, a result that generalizes the findings in [9].

For Gaussian size distributions, Insana and Hall [11] studied the effects of the ratio of the standard deviation σ and mean μ values of the size distribution when obtaining QUS estimates using a solid sphere model for data generation and a rigid sphere model for ESD estimation. They observed that ESD estimates changed as a function of the ka range used for the estimation. Furthermore, they observed that when $ka \approx 0.8$ the ESD estimate corresponded to μ with a bias of less than 10% independently of the σ/μ ratio. Mamou *et al.* [12] briefly studied the effects of increasing the standard deviation of the size distribution on ESD estimates when using a spherical Gaussian scat-

Manuscript received June 24, 2010; accepted December 8, 2010. This work was supported by NIH Grant CA139095.

The authors are with the Department of Electrical and Computer Engineering, University of Illinois at Urbana-Champaign, Urbana, IL (e-mail: lavarell@illinois.edu).

R. Lavarello is also with the Sección Electricidad y Electrónica, Departamento de Ingeniería, Pontificia Universidad Católica del Perú, Lima, Perú.

Digital Object Identifier 10.1109/TUFFC.2011.1867

tering model for both data generation and ESD estimation. Similar to the findings of Insana and Hall, Mamou *et al.* observed that ESD estimates increased with increasing standard deviation of the scatterer size.

Although all of these works reported effects of scatterer size distributions on ESD estimates, none of them have provided a clear description of the effects of continuous size distributions on ESD estimates using different frequency scales. The work in [9] only considered one size distribution realization as a basis for all of the reported conclusions. The work in [10] only presented results with simple discrete size distributions. The works in [11], [12] used Gaussian size distributions, which complicates the ESD estimate analysis because all possible scatterer sizes were present in the imaging targets.

The goal of the present work is to determine if different frequency ranges are indeed more sensitive to different spatial scales when using discrete spherical scatterers with continuous scatterer size distributions of finite support. To that effect, simulations were conducted by constructing computer phantoms with fluid spheres. ESD estimates were obtained for different frequency ranges and their relationship with the underlying size distributions was analyzed. Experiments were also conducted using physical phantoms containing weak scatterers (i.e., Sephadex spheres) to further validate the findings obtained through simulations. In this study, a fluid sphere scattering model was used for consistency between simulation and experimental results. Although the suitability of discrete versus continuous models to describe scattering by tissues is still a subject of debate, the results presented here should have direct applicability for both physical [14] and biological [15] phantom studies.

II. Methods

A. Backscattering by a Multiple-Sized Scatterer Population

The exact analytic solution to the scattering of a plane wave of wave number k by a fluid sphere of radius a, compressibility κ, and density ρ embedded in a fluid medium has been previously reported in the literature [16]. Under weak scattering assumptions, the backscattering cross-section (BCS) $\sigma(k,a)$ in the far-field corresponding to this scattering problem can be written as [17]

$$\sigma(k,a) = \frac{4\pi a^2}{9}(\gamma_\kappa - \gamma_\rho)^2 (ka)^4 \left(\frac{3}{2ka} j_1(2ka) \right)^2, \qquad (1)$$

where $\gamma_\kappa = (\kappa - \kappa_0)/\kappa_0$ and $\gamma_\rho = (\rho - \rho_0)/\rho$ are the fractional changes in κ and ρ, respectively, and $j_1(\cdot)$ is the first-order spherical Bessel function. For illustration, the BCS $\sigma(k,a)$ corresponding to a sphere with $a(\gamma_\kappa - \gamma_\rho) = 1$ is shown in Fig. 1.

One can now consider the situation in which ultrasound is scattered by an ensemble of β scatterers per unit of volume distributed spatially at random in an otherwise homogeneous, fluid medium. Assuming no multiple scattering among the individual scatterers, and neglecting the effects of coherent scattering, the theoretical differential backscattering coefficient (BSC) $\eta(k)_{\text{th}}$ can be expressed as

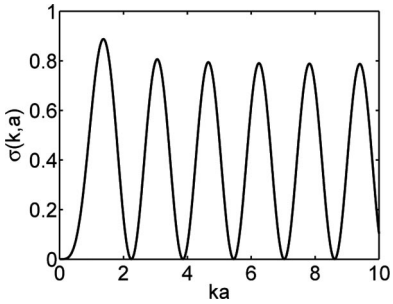

Fig. 1. Backscattering cross-section $\sigma(k,a)$ corresponding to a sphere with $a(\gamma_\kappa - \gamma_\rho) = 1$.

$$\eta(k)_{\text{th}} = \frac{\beta}{4\pi} \int_0^\infty p(a)\sigma(k,a)\mathrm{d}a, \qquad (2)$$

where $p(a)$ is the sphere radius probability distribution function (PDF), i.e., the probability that the sphere radius takes the value a.

B. BSC Estimates From Pulse-Echo Data

To obtain BSC estimates, an acoustic aperture receives pulse-echo pressure waveforms $s_m(t)$ when located at positions $y = y_m$. The BSC can be estimated from the backscattered data from a region of interest (ROI) gated axially between depths $(F - \Delta z/2)$ and $(F + \Delta z/2)$ using a rectangular window, where F is the transducer's focal depth and Δz is the gate length. The normalized backscattered power spectrum $\bar{S}(k)$ is defined here as

$$\bar{S}(k) = \gamma^2 \frac{\langle |S_m(k)|^2 \rangle}{|S_0(k)|^2} F(k), \qquad (3)$$

where $|S_0(k)|^2$ is a reference power spectrum obtained from a reflection off a planar surface of known pressure reflection coefficient γ, $\langle |S_m(k)|^2 \rangle$ is the average of the power spectra of several adjacent, gated scan lines $s_m(t)$, and $F(k)$ is a function that compensates for attenuation effects [18]. The normalized spectrum $\bar{S}(k)$ can be related to BSCs after properly compensating for the transducer diffraction pattern. Following the method in [19], the estimated BSCs $\eta(k)_{\text{est}}$ can be calculated as

$$\begin{aligned} \eta(k)_{\text{est}} &= 2.174 |D_{\text{ref}}(k)| \frac{F^2}{A_0 \Delta z} \bar{S}(k) \\ D_{\text{ref}}(k) &= \exp(-iG_{\text{p}})[J_0(G_{\text{p}}) + iJ_1(G_{\text{p}})] - 1, \end{aligned} \qquad (4)$$

where $A_0 = \pi R^2$ and $G_{\text{p}} = kR^2/2F$ are the aperture area and pressure gain factor of the transducer of radius R, respectively, and $J_m(\cdot)$ is the mth-order Bessel function.

C. Effective Scatterer Diameter Estimation

Microstructural information about the illuminated region can be obtained from estimates of $\eta(k)$. ESD estimates were obtained by minimizing the function [17], [20]

$$\begin{aligned} \mathrm{ESD} &= 2\arg\min_{a}\int_{k_{\min}}^{k_{\max}}(X(k,a)-\bar{X})^2\mathrm{d}k, \\ X(k,a) &= 10\log_{10}(\eta(k)_{\mathrm{est}}/\sigma(k,a)), \end{aligned} \tag{5}$$

where $\bar{X}$ is the mean value of $X(f)$ within the wave number analysis bandwidth $k \in [k_{\min}, k_{\max}]$.

D. ESD Estimation Simulations

Two continuous scatterer size distributions were analyzed in this study. The first case corresponded to a uniform distribution, i.e.,

$$p(a) = \begin{cases} \frac{1}{a_{\max}-a_{\min}}, & a \in [a_{\min}, a_{\max}] \\ 0, & \text{else.} \end{cases} \tag{6}$$

The second case corresponded to an inverse cubic distribution, i.e.,

$$p(a) = \begin{cases} \frac{2}{a_{\min}^{-2}-a_{\max}^{-2}}\frac{1}{a^3}, & a \in [a_{\min}, a_{\max}] \\ 0, & \text{else.} \end{cases} \tag{7}$$

The rationale behind the inverse cubic distribution was that the number of spheres of radius a that could be fit into a fixed volume V decreases as $1/a^3$. Therefore, there are more likely to be a larger number of smaller scatterers contained in a particular volume than larger scatterers. It should be emphasized at this point that given the current lack of knowledge about actual scattering sites in tissues, it is not suggested here that these distributions are necessarily representative of the ones found in biomedical QUS applications. However, it is expected that given the rather dissimilar emphasis the PDFs used in this study give to small scatterers [i.e., the ones with lower associated $\sigma(k, a)$ amplitudes] the results presented here will provide insights into the effect of general continuous scatterer size distributions. For all simulations, the individual scatterers were modeled as weakly scattering fluid spheres with $(\gamma_\kappa - \gamma_\rho) = 0.1$. Four different ranges of scatterer diameters were used in the simulations: 25 to 100 μm, 25 to 50 μm, 50 to 100 μm, and 50 to 75 μm. The effects of scatterer size distributions were studied by conducting simulations using two methods:

1) Method 1: In the first method, (2) was used to calculate $\eta(k)_{\mathrm{th}}$ for several frequencies between 0 and 60 MHz using $p(a)$ as given by either (6) or (7). The evaluation of (2) was performed using numerical quadrature integration. Afterwards, ESD estimates were obtained using (5) with $\eta(k)_{\mathrm{est}} = \eta(k)_{\mathrm{th}}$. ESD estimates at different frequencies f_0 were obtained by analyzing the synthetic BSCs between $f_{\min} = 0.5f_0$ and $f_{\max} = 1.5f_0$, i.e., assuming an imaging system with 100% useable fractional bandwidth.

2) Method 2: The second method for evaluating the effects of size distributions consisted of simulating RF data and using (4) to calculate $\eta(k)_{\mathrm{est}}$ for several ROIs of axial and lateral sizes of 16 λ (with λ calculated using the transducer center frequency) and 4 lateral beamwidths, respectively. The mean and standard deviation of the estimated ESD values obtained with simulated $f/4$ transducers of center frequencies equal to 3, 6, 12, 24, and 36 MHz and 100% −6-dB fractional bandwidth (which resulted in −6-dB pulse lengths of approximately $\lambda/2$) were calculated. Special care was taken to ensure the scatterers did not overlap when generating the computer phantoms used for the RF data simulations. The number of scatterers per resolution cell was set to 80 considering the 3-MHz simulated transducer, and the same phantoms were imaged using all five simulated transducers to isolate the effects of different imaging frequency ranges. The scatterer concentration was set to a moderate value at the low-frequency end to avoid issues associated with large scatterer volume fractions [21]. It should be noted, however, that at the highest center frequency considered in the simulations there were only approximately 6 scatterers per ROI (i.e., $32 \times 4 = 128$ resolution cells per ROI with $80/12^3$ scatterers per resolution cell at 36 MHz), and therefore coherent scattering effects may be observed for increasing analysis frequencies.

For both methods, the minimization of the expression in (5) was conducted by performing an extensive search considering ESDs in the range between 1 and 180 μm.

E. ESD Estimation Experiments

Experimental results were obtained by constructing 250 bloom-strength, Type-B gelatin (Rousselot Inc., Dubuque, IA) phantoms. The background gelatin mixture consisted of 12% w/w gelatin powder, 87% de-ionized water, and 1% Germall Plus. The density and speed of sound of the gelatin mixture were measured to be 1.02 g/mL and 1.54 mm/μs, respectively. Scattering was produced using Sephadex spheres (Sephadex G-25 Fine, GE Healthcare, Chalfont St. Giles, UK) at a concentration of 2 g of dry spheres per 400 mL of gelatin mixture. The Sephadex spheres were soaked in distilled water for 24 h before making the phantom, as recommended in [11]. The mass density of Sephadex was measured to be 1.3 g/mL. In this work, it was assumed that no sound speed contrast existed between the Sephadex spheres and the gelatin background. The manufacturer reported a wet particle diameter ranging between 35 and 140 μm. Two phantoms were constructed. The first phantom contained spheres spanning the whole range provided by the manufacturer. The second phantom was constructed using Sephadex spheres sieved before wetting to have a diameter larger than 53 μm. For both phan-

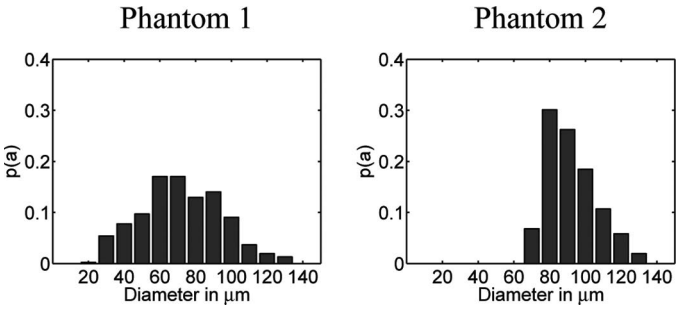

Fig. 2. Scatterer size PDF $p(a)$ corresponding to the first (left) and second (right) phantoms used for the experimental BSC measurements.

toms, a portion of the gelatin plus Sephadex mixture was preserved, sliced, and imaged using an optical microscope for sphere size determination. The scatterer size PDF estimates for both phantoms are given in Fig. 2.

Four different transducers with nominal center frequencies of 5, 7.5, 10, and 13 MHz were used to scan the phantom. The properties of the transducers used for the experiments are given in Table I. A total of 441 scan lines were obtained by translating a transducer over an area of 4 cm^2. Spectra from segments of length $\Delta z = 15\lambda$ centered around the transducer focus, with λ calculated using the nominal transducer center frequency, were obtained for all 441 scan lines. All 441 estimated spectra were combined to obtain an average BSC curve for each transducer. Attenuation compensation was performed using [18, Eq. (16)] with the attenuation coefficients of each phantom estimated using through-transmission measurements with an f/4, 7.5-MHz transducer and fitted to a cubic polynomial. The estimated ESD was obtained using (5) and performing an extensive search considering ESDs in the range between 1 and 240 μm.

III. Results

A. Simulation Results

The simulation results are presented in Figs. 3 and 4 for the uniform and inverse cubic size distributions, respectively. In both figures, the top row presents the BSCs corresponding to the scatterer populations (normalized to a maximum value of 1 for the presented frequency range) as predicted by (2), and the bottom row presents the ESD estimates using method 1 (solid line) and method 2 (star marks with error bars). For all simulations, there is an agreement between the ESD estimates predicted by the two simulation methods. Therefore, any potential coher-

TABLE I. Properties of the Transducers Used for the Experimental BSC Measurements.

Nominal center frequency (MHz)	Analysis bandwidth (MHz)	f/#	Diameter
5	2.4 to 7.0	3	0.75 in (19.05 mm)
7.5	3.5 to 11.0	4	0.75 in (19.05 mm)
10	5.2 to 16.1	4	0.5 in (12.7 mm)
13	7.5 to 19.2	3	0.5 in (12.7 mm)

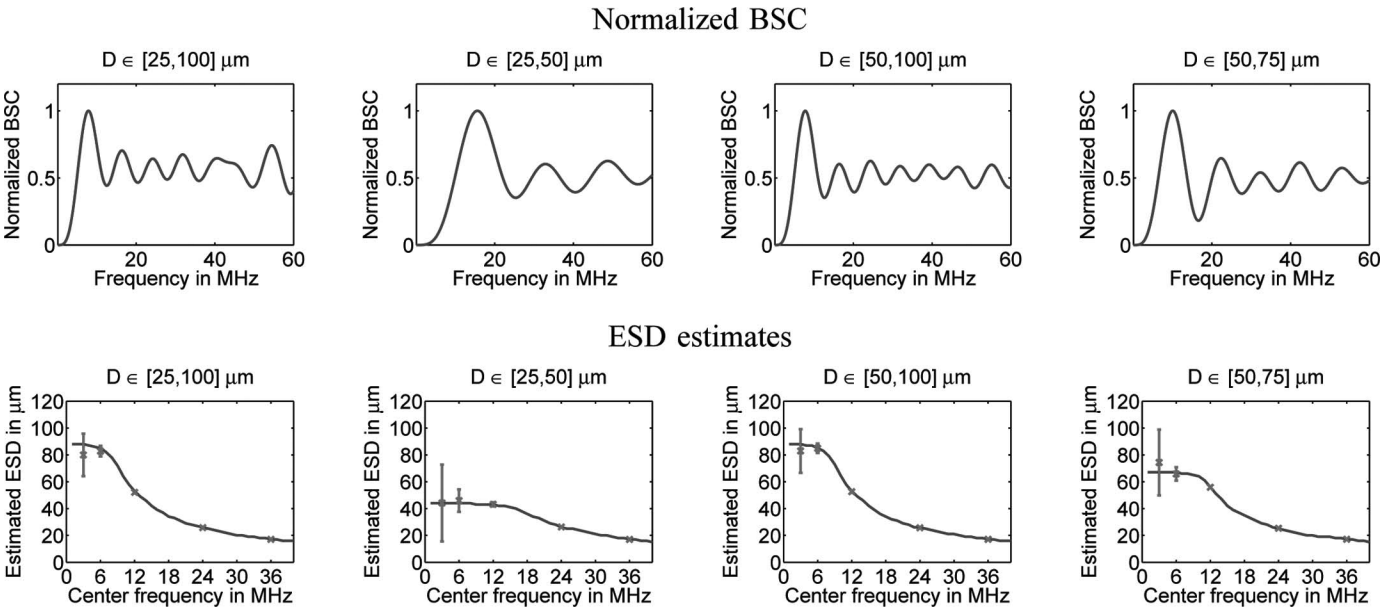

Fig. 3. Simulation results using a uniform scatterer size distribution. Top row: normalized BSCs as predicted by (2). Bottom row: ESD estimates obtained using methods 1 (solid line) and 2 (star marks with error bars).

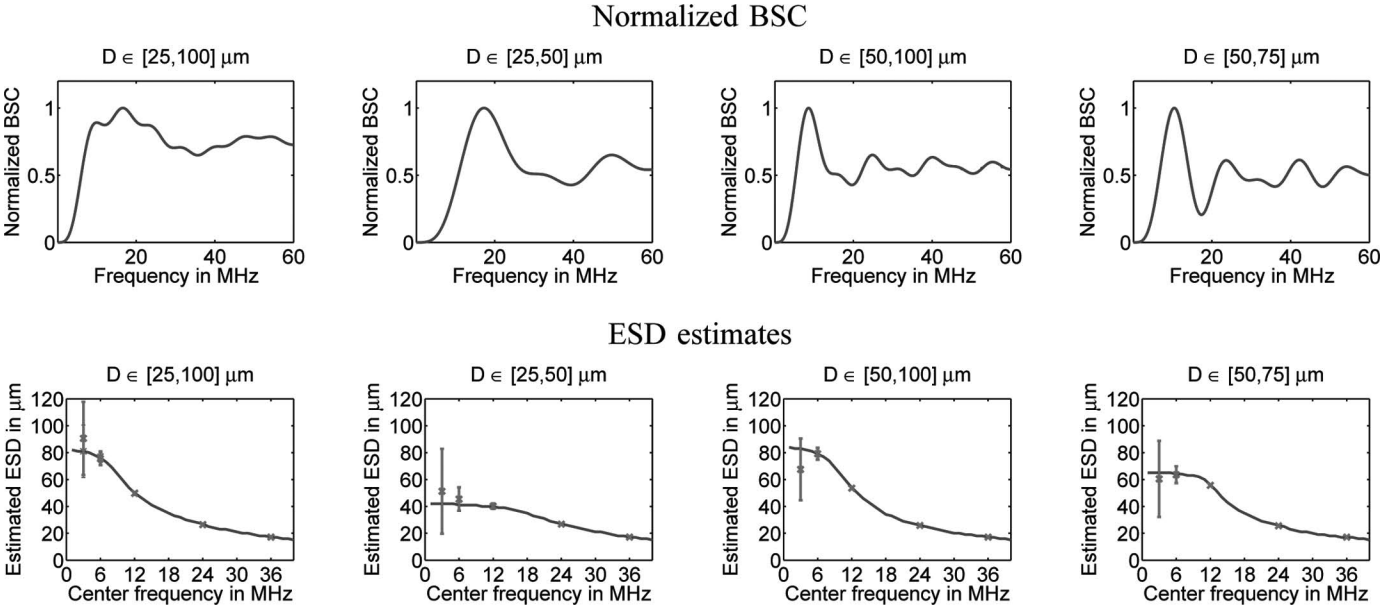

Fig. 4. Simulation results using an inverse cubic scatterer size distribution. Top row: normalized BSCs as predicted by (2). Bottom row: ESD estimates obtained using methods 1 (solid line) and 2 (star marks with error bars).

ent effects in the estimated BSCs when using simulation method 2 did not influence the estimated ESDs when using the estimation method outlined in Section II-C. It can be observed that both simulation methods predict a decrease in the value of the ESD estimates for increasing center frequency of the analysis range. Consistent with observations reported in the literature, the variance of the ESD estimates obtained using simulation method 2 increased with decreasing analysis frequencies as the dominant ka values were reduced below 1 [11], [22].

B. Experimental Results

The experimental results are presented in Fig. 5. In the first column of Fig. 5, the normalized experimental BSC obtained using the 5-MHz (solid line), 7.5-MHz (dash-dotted line), 10-MHz (dashed line), and 13-MHz (dotted line) transducers, together with the theoretical BSC (thick dotted line) predicted using (2) are presented. The theoretical BSC curves were obtained using (2) together with (1) and the PDFs reported in Fig. 2.

The agreement between the theoretical $\eta_{\text{th}}(k)$ and experimental $\eta_{\text{est}}(k)$ BSC curves was quantified by calculating the mean and standard deviation of the log-error $10\log_{10}(\eta_{\text{est}}(k)/\eta_{\text{th}}(k))$. The log-error mean and standard deviation values were 0.96 dB and 0.37 dB for phantom 1 and −0.43 dB and 0.5 dB for phantom 2, respectively. Therefore, both the magnitude and frequency dependence of the experimental and theoretical BSC curves corresponding to both phantoms were in very good agreement. It should be remarked that ESD estimates depend only on the frequency dependence of estimated BSCs. It can be observed that for phantom 2 (i.e., the phantom with the narrower size distribution) the BSC minimum around 11 MHz is more pronounced than for phantom 1.

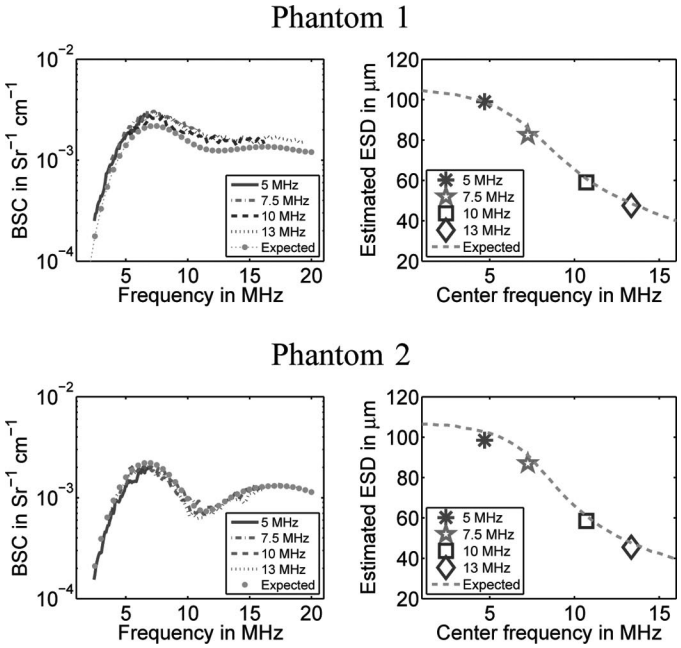

Fig. 5. Experimental results corresponding to the Sephadex sphere phantoms. First column: experimental BSC curves obtained with the 5-, 7.5-, 10-, and 13-MHz transducers. For comparison, the normalized BSCs predicted by theory are also presented. Second column: estimated ESDs obtained with the 5-, 7.5-, 10-, and 13-MHz transducers, together with the theoretical curves predicted using method 1 from Section II-D.

The ESD estimates obtained with the 5-MHz (star), 7.5-MHz (pentagon), 10-MHz (square), and 13-MHz (diamond) transducers, together with the theoretical curve (dashed line) predicted using method 1 from Section II-D, are presented in the second column of Fig. 5. When reporting the experimental ESD estimates, the center frequency was taken to be equal to the mean frequency of the analysis bandwidths reported in Table I. As expected

TABLE II. ESD Estimates (in Micrometers) Obtained From the Sephadex Sphere Phantoms.

Center frequency* (MHz)	Phantom 1		Phantom 2	
	Experiment	Expected	Experiment	Expected
5 (4.7)	99	98.5	98.5	102.5
7.5 (7.25)	82.5	86.0	87.0	91.0
10 (10.7)	59.0	61.0	58.5	61.0
13 (13.35)	47.5	48.5	45.5	47.5

*In the first column, the nominal and analysis band center frequencies are reported outside and inside parentheses, respectively.

TABLE III. Expected ESD Estimates in Micrometers at Low Frequencies.

Diameter range (μm)	Uniform		Inverse cubic	
	Eq. (9)	Simulation	Eq. (10)	Simulation
25 to 100	88.2	88.0	81.8	81.5
25 to 50	44.2	44.0	41.8	42.0
50 to 100	88.5	88.5	83.7	83.5
50 to 75	67.3	67.5	65.3	65.5

from the agreement between theoretical and experimental BSC curves, the experimental and theoretical ESD estimates were in very good agreement. The experimental and expected ESD estimates at the analysis center frequencies of all transducers are reported in Table II.

IV. Discussion

Several important observations can be drawn from the results presented in the previous section. First, the results of Section III-A indicated that for low enough analysis frequencies, the ESD estimates were highly biased by the maximum size of the largest scatterers present. For low analysis frequencies and weakly scattering spherical inclusions, the estimated ESD should converge to (see Appendix)

$$\hat{D} = 2\sqrt{\frac{\int_{a_{\min}}^{a_{\max}} p(a)a^8 \mathrm{d}a}{\int_{a_{\min}}^{a_{\max}} p(a)a^6 \mathrm{d}a}}. \tag{8}$$

For the particular cases of uniform and inverse cubic scatterer size distributions, the low-frequency ESD estimates will be given by

$$\hat{D}_{\mathrm{UD}} = 2\sqrt{\frac{7}{9}\frac{a_{\max}^9 - a_{\min}^9}{a_{\max}^7 - a_{\min}^7}} \tag{9}$$

$$\hat{D}_{\mathrm{ICD}} = 2\sqrt{\frac{2}{3}\frac{a_{\max}^6 - a_{\min}^6}{a_{\max}^4 - a_{\min}^4}}. \tag{10}$$

For the rest of this work, the term "low frequencies" will be reserved to the frequencies that satisfy $k\hat{D}/2 \ll 1$. The expected ESDs at low frequencies corresponding to the populations used in Section III-A are given in Table III.

The simulation results at low frequencies had excellent agreement with the values predicted by (8), as reported in Table III. The bias toward larger scatterers has been reported previously in the literature [11], and was cited by Mamou *et al.* [10] as the reason why the smaller scatterers in a Bernoulli distribution could only be detected using QUS if their acoustic concentration was large enough compared with that of the larger scatterers. It should be noted here that this effect prevailed even for the inverse cubic distribution, which largely emphasized the acoustic concentration of small scatterers.

The expression in (8) was derived by keeping the first two terms of the Taylor series expansion in (15). A different expression was derived in [11] by only keeping the first term in the Taylor expansion in (15), i.e., $\sigma(k,a) \approx k^4 a^6$. Under this assumption, the ESD limit at low ka was proposed to be equal to [11]

$$\bar{D} = 2\left(\int_{a_{\min}}^{a_{\max}} p(a)a^6 \mathrm{d}a\right)^{1/6}. \tag{11}$$

For the cases of uniform and inverse cubic size distributions, (11) reduces to

$$\bar{D}_{\mathrm{UD}} = 2\left(\frac{a_{\max}^7 - a_{\min}^7}{a_{\max} - a_{\min}}\right)^{1/6} \tag{12}$$

$$\bar{D}_{\mathrm{ICD}} = 2\left[\left(\frac{a_{\max}^4 - a_{\min}^4}{2}\right)\left(\frac{a_{\max}^2 a_{\min}^2}{a_{\max}^2 - a_{\min}^2}\right)\right]^{1/6}. \tag{13}$$

However, this approach is not expected to properly predict ESD estimates at low ka because if one only considers the k^4 frequency dependence, then $\sigma(k,a)$ would be the same for all a up to a scaling factor and therefore (5) would not converge. As an example, when using $a_{\min} = 12.5$ μm and $a_{\max} = 50$ μm the expressions in (12) and

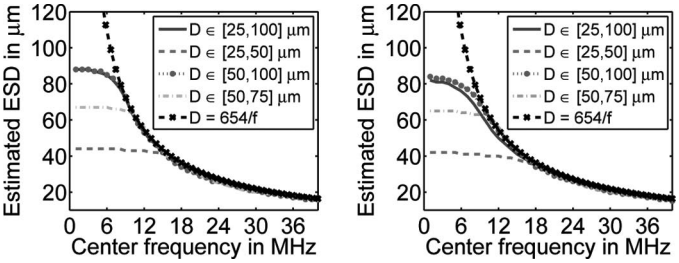

Fig. 6. ESD estimates when using uniform (left) and inverse cubic (right) size distributions.

TABLE IV. PROPORTIONALITY CONSTANT OF THE ASYMPTOTIC $1/f$ ESD BEHAVIOR AT HIGH FREQUENCIES.

Diameter range (μm)	Uniform Eq. (9)	Inverse cubic Eq. (10)
25 to 100	625	611
25 to 50	610	597
50 to 100	625	631
50 to 75	641	644

(13) predict $\bar{D} = 81.1$ μm and $\bar{D} = 56.7$ μm for the uniform and inverse cubic distributions, respectively. In this case, the underestimation of the expected ESD for low ka values when using (11) was moderate for the uniform distribution but significant when using an inverse cubic distribution.

Second, for high frequency values, the ESD estimates decayed monotonically. For further clarification of the behavior of the estimated ESD values as a function of frequency, the ESD curves corresponding to the four populations studied in Section III-A are presented together in Fig. 6 for both scatterer size distributions. It can be observed that all curves closely approached a common asymptotic behavior for high enough frequency values. It is hypothesized here that the asymptotic behavior was caused by the estimator locking onto the first lobe of $\sigma(k, a)$, i.e., the region around the first maximum of $\sigma(k, a)$ at $ka \approx 1.37$ as shown in Fig. 1. This situation arises from the inability of the single-size $\sigma(k, a)$ to reproduce the expected BSC generated by populations of scatterers of different sizes for high enough frequencies, as observed by comparing the BSC curves in Figs. 3 and 4 with $\sigma(k, a)$ in Fig. 1. Insana and Hall [11] also observed and discussed this estimation ambiguity when using oscillatory scattering models in the context of ESD estimation with noisy data. Insana and Hall argued in [11] that the flat frequency response of $\sigma(k, a)$ around its first lobe minimized the variance of $\log(\eta(k)_{\text{est}}/\sigma(k, a))$. For the rest of this work, the term "high frequencies" will be reserved to the frequencies that satisfy $k\hat{D}/2 > 1.37$.

Given that the first lobe is approximately centered around $ka = 1.37$, the diameter D_{AS} that corresponds to locking onto the first lobe of $\sigma(k, a)$ as a function of the center frequency f of the analysis range is given by

$$D_{\text{AS}} \approx \frac{2000 \times 1.37 c_0}{2\pi} \frac{1}{f} = \frac{654}{f}, \tag{14}$$

where c_0 is the speed of sound in the background (considered here to be 1.5 mm/μs), D_{AS} is given in micrometers, and f is given in megahertz. The asymptotic curve corresponding to (14) is also plotted in Fig. 6. It can be observed that for both distributions, the asymptotic curve agrees very well with the ESD estimates for sufficiently high analysis frequencies.

It should be stressed the expression in (14) is only an approximation of the actual frequency dependence of the ESD estimates. To compare (14) with the simulation results, ESD curves obtained with method 1 from Section II-D were fitted to $1/f$ in the range between 24 and 54 MHz. The proportionality constants obtained from a least mean square fit for all cases reported in Section III-A are shown in Table IV. The obtained proportionality constants are all within 10% of the value of 654 estimated from the location of the first peak of the scattering model function in (1). Deviations from the expression in (14) are expected because the actual size distribution has an effect on the shape of the BSC curves, as can be assessed from Figs. 3 and 4. Although the actual scatterer size distribution will have some effect on the ESD estimates obtained when using (5), the results presented in this work suggest such dependence will be very weak and (14) can be used as a good approximation to describe the behavior of ESD estimates for high enough frequencies.

Given that the asymptotic behavior of ESD curves is almost independent of the actual scatterer size distribution, these results suggest that ESD estimates may fail to represent actual microstructural properties of the analyzed ROIs if scattering is described using a single scatterer model. In particular, Fig. 6 showed that at 36 MHz, the estimated ESDs were around 20 μm for all of the analyzed distributions even though the smallest scatterers for two of the four analyzed populations were 50 μm in diameter. Further, for all simulations the standard deviations of the ESD estimates using method 2 were less than 4% of the corresponding mean ESD values at 12 MHz and above, which could erroneously be interpreted as a sign of robust estimations.

Third, the results presented in Section II-B suggest that the trends observed in simulations may also be observed in experiments. In particular, two key results have been experimentally validated. First, the experimental ESD versus analysis frequency curves in the first column of Fig. 5 exhibited the same inverse frequency dependence observed in simulations. Further, the curves became almost equivalent to each other for sufficiently high analysis frequencies. Second, and perhaps more importantly, the ESD estimates obtained from phantom 2 using the 10- and 13-MHz transducers were outside the range of scatterer sizes actually present in the phantom and reported in Fig. 2.

The results presented in this study complement earlier works available in the literature. It is worth noting that it is not suggested here that QUS imaging will not be capable of providing meaningful ESD estimates at high frequencies for any scatterer size distribution. Certainly, previous studies have shown that different spatial scales can be resolved when imaging targets with simple discrete bimodal scatterer size distributions (i.e., a Bernoulli distribution) [9]. Similarly, for particular cases of continuous size distributions it should be possible to properly estimate microstructural properties. However, it has already been reported that even for simple discrete bimodal distributions proper determination of microstructure is not guaranteed for all combinations of scatterer sizes and acoustic concentrations [10]. The results presented here are the continuous unimodal distribution counterpart, and suggest that different frequency ranges will not necessarily be sensitive to different spatial scales because of the potential inability of scattering models to properly predict the more complicated estimated BSCs at high frequencies.

Further, it is not suggested here either that ESD estimates are not meaningful representations of microstructural properties. In fact, the results of this study may provide new insights into how to properly interpret ESD estimates. Until now, a recurrent problem of QUS imaging has been the inability to determine the validity of the obtained estimates given that estimators such as the one in (5) will always provide a valid numerical solution. The presented results suggest that analyzing the behavior of the ESD versus frequency curves may provide a way to analyze QUS estimates. Although high-frequency estimates may not be related to actual microstructural properties, comparison with asymptotic ESD curves such as the one presented in Fig. 6 can be used to determine if the obtained QUS estimates are indeed correlated with tissue microstructure. The results presented here suggest that even if QUS estimators are not sensitive to small spatial scales, the ESD estimates at low enough frequencies will be highly correlated with the largest scatterer size present in the interrogated ROIs, which is a meaningful microstructural descriptor.

Finally, it should be acknowledged that it would be preferable if QUS estimators were sensitive enough to provide more information about a general continuous unimodal scatterer size distribution. It is clear from the experimental BSC curves presented in Fig. 5 that the ESD estimator in (5) could not effectively exploit the noticeable shape difference between the BSCs corresponding to the experimental phantoms. Therefore, the results presented here are likely to be dependent also on the optimization problem used for ESD estimation. The goal of more robust ESD estimation may require more elaborate scattering models that include information about typical scatterer size distributions in tissues, as suggested by Insana and Hall [11]. For example, Mamou *et al.* in [12] demonstrated the use of an exponential form factor to estimate the mean μ and standard deviation σ sizes of populations of spherical Gaussian scatterers with Gaussian size distributions [23]. In particular, in simulations using $\mu = 32$ μm and $\sigma = 8$ μm, the two-parameter model allowed estimation of μ with near-zero bias, whereas the use of the simple Gaussian scattering model resulted in ESD estimates around 37 μm. However, in practice, the highly complex relationship between BSCs and scatterer size distributions may cause the inverse problem to become intractable or ill-conditioned.

V. Conclusions

The results presented in this work highlight some of the effects of continuous scatterer size distributions when obtaining ESD estimates. In general, ESD estimates were found to change as a function of the frequency range used for the size estimation. It was observed that for low frequencies, the ESD estimates were highly uniform and biased toward the maximum scatterer size, whereas for high frequencies, the ESD estimates reached asymptotic values almost independent of the actual scatterer size distribution. Therefore, these results challenge the hypothesis that different frequency ranges are more sensitive to different spatial scales when using a single-size scattering model. Although the results presented here are not necessarily universal and most likely will be affected by the actual size distribution, frequency-dependent BCS of the individual scatterers, and the actual algorithm used for ESD estimation, this work suggests that caution must be exerted when analyzing and interpreting ESD estimates over different frequency ranges.

Appendix

Low-frequency ESD estimates from a population of scatterers to obtain asymptotic ESD estimates in the low ka limit, an expansion of $\eta(k,a)$ as $ka \to 0$ must be performed. For low ka values, and using the Taylor expansion of $j_1(x)$ [24], the dependence of $\sigma(k,a)$ in (1) on k and a can be expressed as

$$\sigma(k,a) \propto k^4 a^6 \left[1 + \sum_{m=1}^{\infty} \frac{A_m}{A_0} (ka)^{2m}\right]^2 \qquad A_m = \frac{(-2)^m}{m!(2m+3)!!}. \tag{15}$$

For low ka values, only the term $m = 1$ in (15) needs to be considered. Using the fact that $(1 + x)^n \to (1 + nx)$ for $x \ll 1$, the single scatterer BCS in (15) can be approximated as

$$\sigma(k,a) \propto k^4 a^6 [1 + \chi k^2 a^2] \qquad \chi = \frac{2A_1}{A_0} = -0.8. \tag{16}$$

Therefore, the backscattering coefficient $\eta(k)$ can be written as

$$\begin{aligned}\eta(k) &\propto \int_{a_{\min}}^{a_{\max}} k^4 a^6 (1+\chi k^2 a^2) p(a)\mathrm{d}a \\ &= k^4 \left(\int_{a_{\min}}^{a_{\max}} p(a) a^6 \mathrm{d}a + \chi k^2 \int_{a_{\min}}^{a_{\max}} p(a) a^8 \mathrm{d}a \right) \qquad (17) \\ &\propto k^4 \left[1 + \chi k^2 \left(\frac{\int_{a_{\min}}^{a_{\max}} p(a) a^8 \mathrm{d}a}{\int_{a_{\min}}^{a_{\max}} p(a) a^6 \mathrm{d}a} \right) \right].\end{aligned}$$

The use of the expressions in (16) and (17) together with the estimator in (5) results in the expression given by (8).

Acknowledgments

The authors would like to thank Dr. M. Insana for useful discussions, and K. Hall, R. Miller, J. Blue, and Dr. G. Ghoushal for technical assistance.

References

[1] E. J. Feleppa, F. L. Lizzi, D. J. Coleman, and M. M. Yaremko, "Diagnostic spectrum analysis in ophthalmology: A physical perspective," *Ultrasound Med. Biol.*, vol. 12, no. 8, pp. 623–631, Aug. 1986.

[2] E. J. Feleppa, A. Kalisz, J. B. Sokil-Melgar, F. L. Lizzi, T. Liu, A. L. Rosado, M. C. Shao, W. R. Fair, Y. Wang, M. S. Cookson, V. E. Reuter, and W. D. W. Heston, "Typing of prostate tissue by ultrasonic spectrum analysis," *IEEE Trans. Ultrason. Ferroelectr. Freq. Control*, vol. 43, no. 4, pp. 609–619, Jul. 1996.

[3] M. F. Insana, T. J. Hall, and J. L. Fishback, "Identifying acoustic scattering sources in normal renal parenchyma from the anisotropy in acoustic properties," *Ultrasound Med. Biol.*, vol. 17, no. 6, pp. 613–626, 1991.

[4] F. L. Lizzi, D. L. King, M. C. Rorke, J. Hui, M. Ostromogilsky, M. M. Yaremko, E. J. Feleppa, and P. Wai, "Comparison of theoretical scattering results and ultrasonic data from clinical liver examinations," *Ultrasound Med. Biol.*, vol. 14, no. 5, pp. 377–385, 1988.

[5] M. L. Oelze, W. D. O'Brien Jr., J. P. Blue, and J. F. Zachary, "Differentiation and characterization of rat mammary fibroadenomas and 4T1 mouse carcinomas using quantitative ultrasound imaging," *IEEE Trans. Med. Imaging*, vol. 23, no. 6, pp. 764–771, Jun. 2004.

[6] W. Liu and J. A. Zagzebski, "Trade-offs in data acquisition and processing parameters for backscatter and scatterer size estimations," *IEEE Trans. Ultrason. Ferroelectr. Freq. Control*, vol. 57, no. 2, pp. 340–352, Feb. 2010.

[7] A. L. Gerig, T. Varghese, and J. A. Zagzebski, "Improved parametric imaging of scatterer size estimates using angular compounding," *IEEE Trans. Ultrason. Ferroelectr. Freq. Control*, vol. 51, no. 6, pp. 708–715, Jun. 2004.

[8] T. A. Bigelow, M. L. Oelze, and W. D. O'Brien Jr., "Estimation of total attenuation and scatterer size from backscattered ultrasound waveforms," *J. Acoust. Soc. Am.*, vol. 117, no. 3, pt. 1, pp. 1431–1439, Mar. 2005.

[9] V. Roberjot, S. L. Bridal, P. Laugier, and G. Berger, "Absolute backscatter coefficient over a wide range of frequencies in a tissue-mimicking phantom containing two populations of scatterers," *IEEE Trans. Ultrason. Ferroelectr. Freq. Control*, vol. 43, no. 5, pp. 970–978, Sep. 1996.

[10] J. Mamou, M. L. Oelze, W. D. O'Brien Jr., and J. F. Zachary, "Identifying ultrasonic scattering sites from three-dimensional impedance maps," *J. Acoust. Soc. Am.*, vol. 117, no. 1, pp. 413–423, Jan. 2005.

[11] M. F. Insana and T. J. Hall, "Parametric ultrasound imaging from backscatter coefficient measurements: Image formation and interpretation," *Ultrason. Imaging*, vol. 12, no. 4, pp. 245–267, Oct. 1990.

[12] J. Mamou, M. L. Oelze, W. D. O'Brien Jr., and J. F. Zachary, "Extended three-dimensional impedance map methods for identifying ultrasonic scattering sites," *J. Acoust. Soc. Am.*, vol. 123, no. 2, pp. 1195–1208, Feb. 2008.

[13] J. J. Faran Jr., "Sound scattering by solid cylinders and spheres," *J. Acoust. Soc. Am.*, vol. 23, no. 4, pp. 405–418, Jul. 1951.

[14] K. A. Wear, T. A. Stiles, G. R. Frank, E. L. Madsen, F. Cheng, E. J. Feleppa, C. S. Hall, B. S. Kim, P. Lee, W. D. O'Brien Jr, M. L. Oelze, B. I. Raju, K. K. Shung, T. A. Wilson, and J. R. Yuan, "Interlaboratory comparison of ultrasonic backscatter coefficient measurements from 2 to 9 MHz," *J. Ultrasound Med.*, vol. 24, no. 9, pp. 1235–1250, Sep. 2005.

[15] R. E. Baddour, M. D. Sherar, J. W. Hunt, G. J. Czarnota, and M. C. Kolios, "High-frequency ultrasound scattering from microspheres and single cells," *J. Acoust. Soc. Am.*, vol. 117, no. 2, pp. 934–943, Feb. 2005.

[16] V. C. Anderson, "Sound scattering from a fluid sphere," *J. Acoust. Soc. Am.*, vol. 22, no. 4, pp. 426–431, Jul. 1950.

[17] M. F. Insana, R. F. Wagner, D. G. Brown, and T. J. Hall, "Describing small-scale structure in random media using pulse-echo ultrasound," *J. Acoust. Soc. Am.*, vol. 87, no. 1, pp. 179–192, Jan. 1990.

[18] M. L. Oelze and W. D. O'Brien Jr., "Frequency-dependent attenuation-compensation functions for ultrasonic signals backscattered from random media," *J. Acoust. Soc. Am.*, vol. 111, no. 5, pt. 1, pp. 2308–2319, May 2002.

[19] X. Chen, D. Phillips, K. Q. Schwarz, J. G. Mottley, and K. J. Parker, "The measurement of backscatter coefficient from a broadband pulse-echo system: A new formulation," *IEEE Trans. Ultrason. Ferroelectr. Freq. Control*, vol. 44, no. 2, pp. 515–525, Mar. 1997.

[20] M. L. Oelze, J. F. Zachary, and W. D. O'Brien Jr., "Characterization of tissue microstructure using ultrasonic backscatter: Theory and technique for optimization using a Gaussian form factor," *J. Acoust. Soc. Am.*, vol. 112, no. 3, pt. 1, pp. 1202–1211, Sep. 2002.

[21] J.-F. Chen and J. A. Zagzebski, "Frequency dependence of backscatter coefficient versus scatterer volume fraction," *IEEE Trans. Ultrason. Ferroelectr. Freq. Control*, vol. 43, no. 3, pp. 345–353, May 1996.

[22] P. Chaturvedi and M. F. Insana, "Error bounds on ultrasonic scatterer size estimates," *J. Acoust. Soc. Am.*, vol. 100, no. 1, pp. 392–399, Jul. 1996.

[23] J. Mamou, "Ultrasonic characterization of three animal mammary tumors from three-dimensional acoustic tissue models," Ph.D. dissertation, Electrical and Computer Engineering Dept., University of Illinois at Urbana-Champaign, 2005.

[24] M. Abramowitz and I. A. Stegun, *Handbook of Mathematical Functions with Formulas, Graphs, and Mathematical Tables*. Mineola, NY: Dover, 1972.

Roberto Lavarello was born in Lima, Perú, in 1978. He earned his B.S. degree in electronic engineering in 2000 from the Pontificia Universidad Católica del Perú, Lima, Perú, and his M.S. and Ph.D. degrees in electrical and computer engineering from the University of Illinois at Urbana-Champaign in 2005 and 2009, respectively. Dr. Lavarello was a Fulbright scholarship recipient from 2003 to 2005. From 2009 to 2011, Dr. Lavarello was a post-doctoral researcher at the University of Illinois at Urbana-Champaign conducting research in ultrasound. Currently, Dr. Lavarello is an assistant professor in the Sección Electricidad y Electrónica at the Pontificia Universidad Católica del Perú. His research interests include ultrasonic imaging, computational methods for acoustic propagation, quantitative ultrasound, and inverse problems with emphasis on acoustical inverse scattering. He is a member of IEEE and IEEE UFFC.

Michael Oelze was born in Hamilton, New Zealand in 1971. He earned his B.S. degree in physics and mathematics in 1994 from Harding University, Searcy, AR, his M.S. degree in physics in 1996 from the University of Louisiana at Lafayette, Lafayette, LA, and his Ph.D. degree in physics in 2000 from the University of Mississippi, Oxford, MS. Dr. Oelze was a post-doctoral fellow at the University of Illinois at Urbana-Champaign from 2000 to 2004 conducting research in ultrasound. Currently, Dr. Oelze is an assistant professor in the Department of Electrical and Computer Engineering at the University of Illinois at Urbana-Champaign. His research interests include the acoustic interaction with soil, ultrasound tissue characterization, quantitative ultrasound, ultrasound bioeffects, ultrasound tomography techniques, ultrasound therapy, and application of coded excitation to ultrasound imaging. Dr. Oelze is a member of the ASA, a senior member of IEEE and IEEE UFFC, and a fellow of the AIUM.